The Sundowner Winds Experiment (SWEX) Pilot Study: Understanding Downslope Windstorms in the Santa Ynez Mountains, Santa Barbara, California

LEILA CARVALHO,[a,b] GERT-JAN DUINE,[b] CHARLES JONES,[a,b] KATELYN ZIGNER,[a] CRAIG CLEMENTS,[c] HEATHER KANE,[c] CHLOE GORE,[c] GARRET BELL,[a] BRANDI GAMELIN,[a] DAVE GOMBERG,[d] TODD HALL,[d] MARK JACKSON,[d] JOHN DUMAS,[d] ERIC BOLDT,[d] ROB HAZARD,[e] AND WOODY ENOS[e]

[a] Department of Geography, University of California, Santa Barbara, Santa Barbara, California [b] Earth Research Institute, University of California, Santa Barbara, Santa Barbara, California [c] Department of Atmospheric Sciences, San José State University, San Jose, California [d] National Weather Service, Los Angeles and Oxnard, California [e] Santa Barbara County Fire Department, Santa Barbara, California

(Manuscript received 19 June 2019, in final form 15 January 2020)

ABSTRACT

Sundowner winds are downslope gusty winds often observed on the southern slopes of the Santa Ynez Mountains (SYM) in coastal Santa Barbara (SB), California. They typically peak near sunset and exhibit characteristics of downslope windstorms through the evening. They are SB's most critical fire weather in all seasons and represent a major hazard for aviation. The Sundowner Winds Experiment Pilot Study was designed to evaluate vertical profiles of winds, temperature, humidity, and stability leeward of the SYM during a Sundowner event. This was accomplished by launching 3-hourly radiosondes during a significant Sundowner event on 28–29 April 2018. This study showed that winds in the lee of the SYM exhibit complex spatial and temporal patterns. Vertical profiles showed a transition from humid onshore winds from morning to midafternoon to very pronounced offshore winds during the evening after sunset. These winds accompanied mountain waves and a northerly nocturnal lee jet with variable temporal behavior. Around sunset, the jet was characterized by strong wind speeds enhanced by mountain-wave breaking. Winds weakened considerably at 2300 PDT 29 April but enhanced dramatically at 0200 PDT 29 April at much lower elevations. These transitions were accompanied by changes in stability profiles andin the Richardson number.A simulationwith the Weather Research and Forecasting (WRF) Model at 1-km grid spacing was examined to evaluate the skill of the model in capturing the observed winds and stability profiles and to assess mesoscale processes associated with this event. These results advanced understanding on Sundowner's spatiotemporal characteristics and driving mechanisms.

1. Introduction

Coastal Santa Barbara County (SB), with a population exceeding 130000 inhabitants, is among the most exposed communities to wildfire hazards in southern California (Kolden and Abatzoglou 2018). The Santa Ynez Mountains (SYM) rise abruptly from coastal SB separating the Pacific Ocean on its south face from the Santa Ynez Valley (SYV) on its north face. Downslope, dry and gusty windstorms are frequently observed on the southern-facing slopes of the SYM. These winds typically intensify from early evening to morning hours and are known as ''Sundowner winds'' or ''Sundowners'' (Ryan 1996; Blier 1998).

All major wildfires affecting SB coast have exhibited significant fire spread rates toward the SB wildlandurban interface due to Sundowners. Some dramatic examples of these rapidly spreading wildfires fueled by strong Sundowners are: Eagle Canyon (September 1979), Painted Cave (June 1990), Gap (July 2008), Tea-House (November 2008), Jesusita (May 2009), Sherpa (June 2016), Whittier (July 2017), and Thomas Fire ignited in Santa Paula (Ventura County) during persistent Santa Ana winds with gusts as high as 35ms[21]

Supplemental information related to this paper is available

Corresponding author: Leila M. V. Carvalho, leila@eri.ucsb.edu

at the Journals Online website: https://doi.org/10.1175/MWRD-19-0207.s1.

DOI: 10.1175/MWR-D-19-0207.1

(Fovell and Gallagher 2018), the Thomas Fire further spread toward Montecito, SB, on the evening of 16 December due to the strong Sundowner winds (Kolden and Abatzoglou 2018). According to the California Department of Forestry and Fire Protection, these tragic events have caused injuries and fatalities, destroyed hundreds of properties and cost millions of dollars in suppression efforts. Additionally, they led to massive evacuations and disruption of schools and businesses, created unbearable air pollution and environmental problems, among many other issues. Therefore, improved weather warnings of these events, including greater lead time and spatiotemporal specificity of where winds will be strongest is critical in supporting a rapid response in case of a wildfire.

Despite the importance of Sundowners, little is known about the spatiotemporal variability and mechanisms driving these events. Contrary to Santa Ana winds that prevail during fall and winter seasons (Hughes and Hall 2010; Jones et al. 2010), Sundowners occur year round though appear more frequent during spring (Hatchett et al. 2018). Blier (1998) noticed that significant crossmountain flow over the SYM ridgeline is necessary for strong offshore (northerly) winds to erode the marine boundary layer that typically exists. That study also showed that multiple synoptic conditions can lead to strong cross-mountain winds, and suggested that these forcings maybe seasonally dependent. The multiplicity of synoptic settings conducive to Sundowners was also identified in Cannon et al. (2017) based on case studies, some of them related to major wildfires (such as the Painted Cave and Jesusita fires). Ryan (1996) found that strong mean sea level pressure (MSLP) differences between Santa Maria (KSMX) and Santa Barbara
(KSBA) airports are significantly associated with strong Sundowners (typically with a N-NW direction) in the lee of the western section of the SYM. Sukup (2013) noticed that MSLP differences between KSBA and Bakersfield airports (KBFL) could be a better predictor for the N-NE Sundowner winds that typically affect the eastern parts of the SYM.

The National Weather Service Office in Oxnard (hereafter, NWS LOX) considers a significant Sundowner event when atmospheric conditions favor cross-mountain (offshore) winds with sustained wind speeds $30 mph ($13.4 m s^{21}) and/or gusts $35 mph (15.6 m s^{21}) in stations leeward of the SYM. The NWS LOX has utilized the pressure difference criteria (Ryan 1996; Sukup 2013) as a rule of thumb to forecast Sundowners. While MSLP differences have been successfully used in forecasting the potential for Sundowners on synoptic time scales, these measures alone are not sufficient to predict mesoscale features such as the onset and end of stronggusts, spatiotemporalvariability of windsleewardof the SYM, and mountain waves that can enhance windstorms posing significant hazards to aviation. Moreover, the existing network of surface stations and the wind profiler installed at KSBA, though useful in evaluating local conditions, are insufficient to examine mechanisms explaining the observed wind variability downwind of the SYM and in coastal SB. KSBA is located near the coast and is often influenced by a stable and cool marine boundary layer (MBL) that significantly influences winds near ground level. Consequently, significant gradients in winds exist between the coast and foothills of the SYM during Sundowners (Duine et al. 2019). For example, Hatchett et al. (2018) evaluated a climatology of Sundowner events (1979–2014) using KSBA and could not properly identify the remarkable Sundowner event that affected eastern SB and Montecito during the Jesusita Fire (May 2009). That event was clearly detectable in other stations on the SYM slopes (Cannon et al. 2017) and widely recognized by the NWS LOX and local meteorologists. These results demonstrate the large degree of spatial variability of Sundowners and suggest the strong control of the MBL on temperature and winds near ground level (Duine et al. 2019).

Numerous observational and modeling studies have been proposed to explain the dynamics of downslope winds in Alpine-type of mountains (Klemp and Lilly 1975; Smith 1979, 1985; Durran and Klemp 1987; Durran 1990; Gallus and Klemp 2000; Durran 2003; Vosper 2004; Grubisic´ and Billings 2007, 2008; Jiang and Doyle 2008; Lawson and Horel 2015). However, few investigations have been conducted to understand the interaction between downslope winds and a stable and cool MBL in coastal ranges with moderate elevations, which is typically observed in SB and other coastal areas in California. Additionally, upstream conditions such as the v-shaped SYV and the presence of the San Rafael Mountains with elevations exceeding the highest peaks in the SYM are important features to understand Sundowner winds.

Cannon et al. (2017) investigated dynamical mechanisms associated with significant episodes of Sundowner winds based on simulations with the Weather Research and

Forecasting (WRF) Model at 2-km resolution. They hypothesized that the cross-mountain winds generated gravity waves that further accelerated downwind in the lee of the SYM due to the presence of critical layers (Durran and Klemp 1987; Durran 1990, 2003). They showed that a mean-state critical layer, attributable to wind backing and reversal with height in the lower troposphere above mountain top, could be one possible mechanismrelatedtotheaccelerationofwinds.However, this mechanism could not explain all case-studies investigated in that study. In some situations, selfinduced critical layers (identified with Richardson number less than 0.25) could be important in accelerating downslope winds. Smith et al. (2018a) examined 11 years of WRF simulations at 2-km resolution and argued that Sundowners are associated with a lee slope jet forced by internal gravity wave breaking aloft. They also indicated that the mountain wave is forced by a synoptically driven offshore jet (Dorman and Winant 2000; Rahn et al. 2014) with northnorthwesterly winds that propagates into the SYV fromwesttoeast.Smithetal.(2018a)definedSundowners basedon the magnitude of an index that linearly combines WRF 2-km 10-m meridional wind speed and differences in temperature (with respect to a reference point at 1200m) calculated for each grid point and averaged over the southern slopes of the SYM (Smith et al. 2018b). However, since winds are generally stronger in the western portion of the SYM and temperature differences are generally smaller than the wind magnitudes, that approach is skewed by events that are strongly influenced by the offshore jet. Conversely, Cannon et al. (2017) and Duine et al. (2019) investigated case studies that showed stronger winds in the eastern SYM relative to the western SYM slopes, suggesting that multiple mechanisms may influence Sundowner winds.

While the results based on previous numerical simulations seem plausible, observations of winds, temperature and stability profiles are necessary to further characterize the spatiotemporal variability of Sundowners and evaluate their mechanisms, including self-induced wave breaking near mountain top and the lee slope jet discussed in Cannon et al. (2017), Smith et al. (2018a), and Duine et al. (2019). The Sundowner Wind Experiment pilot study (SWEX-P) was designed to enhance the understanding of underlying mechanisms explaining the temporal and spatial variability of winds and relationships to the evolution of the boundary layer and nocturnal lee slope jet. The goal of this experiment was to investigate, based on a sequence of radiosonde profiles, the influence of critical layers and wave breaking on the intensification of winds on the slopes of the SYM. This was accomplished by launching radiosondes leeward of the SYM at 3-hourly intervals during a 27-h period preceding, during and after the significant Sundowner event on 28–29 April 2018. Additionally, this study evaluates the performance of WRF 1-km simulations in reproducing the observed profiles and spatial variability of winds. This manuscript is organized as follows. Section 2 discusses the SWEX-P objectives and experiment design and datasets. Section 3 explains the WRF configuration and simulations. Section 4 summarizes the synoptic conditions during SWEX-P. Section 5 provides the main results of the experiment, focusing on observational analyses (section 5a) and simulations (section 5b). A summary and final conclusions are presented in section 6.

2. SWEX-P design and datasets

The SWEX-P was designed to observe vertical profiles of atmospheric variables downstream in coastal SB during the occurrence of Sundowners. This experiment was led by the University of California, Santa Barbara (UCSB) and the Fire Weather Research Laboratory, San José State University (SJSU). SWEX-P also had the assistance and collaboration of the NWS LOX and logistic support of the Santa Barbara County Fire Department. The California State University Mobile Atmospheric Profiling System (CSU-MAPS) (Clements and Oliphant 2014) was employed to conduct upper-air radiosonde soundings. The following variables were recorded from the boundary layer to the mid- to high troposphere: temperature (8C), relative humidity (%), wind speed (ms^{21}), wind direction (degree), altitude (m), and geopotential height (gpm). Pressure (hPa) was estimated based on altitude calculated with global positioning system (GPS).

SWEX-P was conducted on 28–29 April 2018 and planned according to forecasts issued by the NWS LOX of synoptic conditions conducive to cross-mountain winds capable of developing windstorms leeward of the SYM. The focus on springtime was due to the expected high frequency of Sundowners during this season (Hatchett et al. 2018). The radiosonde launching site was located on the foothills of the SYM in the SB County Fire Department Headquarters (34.4518N, 119.7698W, 83m elevation) (‘‘SBHQ,’’ Fig. 1). Time of launches are shown in Table 1.

Additionally, hourly data from nine in situ stations located at distinct elevations on the southern slopes of the SYM (seven) and in the SYV (two) were examined in this study (Fig. 1). Station data were gathered from NWS stations and Remote Automatic Weather Stations (RAWS). They provided hourly values of temperature, relative humidity,

winds and gusts (Table 2). Regrettably, data from the NOAA wind profiler at KSBA were unavailable during SWEX-P.

3. Mesoscale simulations of Sundowner windsduring SWEX-P

Mesoscale simulations during SWEX-P were performed with the WRF Model (v.3.9.1) (Skamarock et al. 2008). Duine et al. (2019) examined the importance of planetary boundary layer (PBL) and land surface model (LSM) schemes in 1-km WRF simulations of Sundowners (and the lee jet) based on case studies. They showed that the choice of PBL parameterization and roughness length (z_0) (Cao and Fovell 2016, 2018) has strong implications for the characteristics of selfinduced wave breaking near the mountaintop and the erosion of the MBL. The WRF configuration included 4 nested domains with 1-km horizontal grid spacing in the innermost domain covering the SYM, the San Rafael Mountains, and coastal SB (Fig. 2). Initial and lateral boundary conditions were derived from ERAInterim reanalysis fields at ;0.78 latitude–longitude (Dee et al. 2011). WRF configuration and physics settings are based on results discussed in Duine et al. (2019) and summarized in Table 3. The simulation was initialized at 1100 PDT 27 April (to allow sufficient spinup time) and ran through 1700 PDT 29 April. Model performance was evaluated using surface stations (Table 2) and vertical profiles. Winds were bilinearly interpolated to the station location and a height correction was applied to the RAWS winds following Cao and Fovell (2016). Vertical profiles were evaluated at the launch site (SBHQ, Fig. 1) nearest grid point.

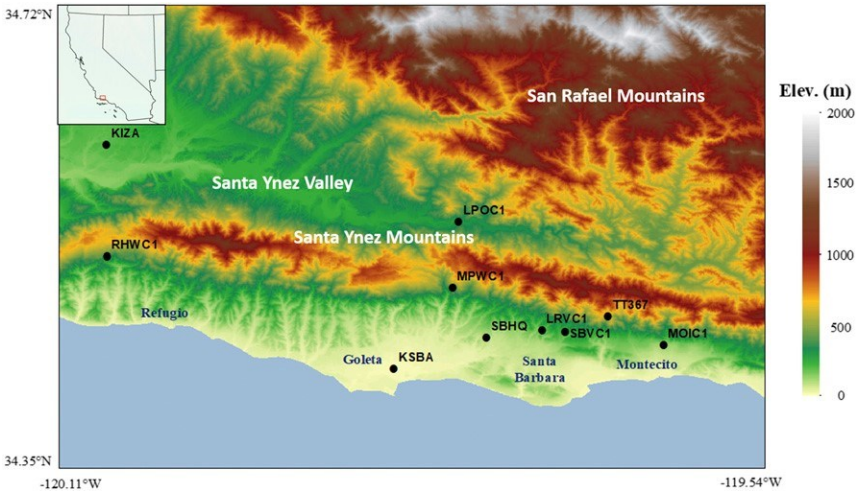

FIG. 1. Santa Barbara County topography (colors) and network of stations (dots) downwind of the Santa Ynez Mountains and in the Santa Ynez Valley reporting winds during SWEX-P. The launching site (SBC Fire Department HQ) is indicated as SBHQ (see Table 2 for details). The approximate location of urban centers (Goleta, Santa Barbara, and Montecito) and Refugio and Gaviota State beaches are included for reference. The inset map indicates the relative position of the domain in the state of California.

4. Synoptic conditions during SWEX-P

The 28–29 April 2018 Sundowner event was characterized by strong synoptic forcing as indicated by the 500-hPa geopotential height and mean sea level pressure obtained from ERA-Interim (Fig. 3). On 28 April, an amplified upper-level trough associated

TABLE 1. Radiosonde launches during SWEX-P: dates (in PDT and UTC), dates used for comparison (PDT), and maximum altitude (m AGL). Radiosondes utilized in this study are DFM-09. Equipment technical characteristics: temperature resolution: 0.18C; temperature accuracy: ,0.28C; relative humidity resolution: 1%; relative humidity accuracy ,4%; pressure accuracy: ,0.3 hPa; geopotential height accuracy: ,20 m; wind speed accuracy: ,0.5 m s^{21}; accuracy horizontal position: ,10 m.

Time (PDT) and date	Time (UTC) and date	Time(PDT) and date (comparisons WRFand stations)	Maximum altitude (m AGL)
0800 28 Apr	1500 28 Apr	0800 28 Apr	18 974.1
1124 28 Apr	1824 28 Apr	1100 28 Apr	23 382.1
1357 28 Apr	2057 28 Apr	1400 28 Apr	23 540.8
1644 28 Apr	2344 29 Apr	1700 28 Apr	24 725.3

1950 28 Apr	0250 29 Apr	2000 28 Apr	25 334.1
2256 28 Apr	0556 29 Apr	2300 28 Apr	11 679.1
0155 29 Apr	0855 29 Apr	0200 29 Apr	14 476.8
0457 29 Apr	1157 29 Apr	0500 29 Apr	7752.1
0747 29 Apr	1447 29 Apr	0800 29 Apr	22 456.4
1100 29 Apr	1800 29 Apr	1100 29 Apr	21 451.8

TABLE 2. Station name, location, coordinates, elevation, and collecting agency (stations in Fig. 1). Stations on the southern slopes of the SYM are indicated in bold. RAWS winds are observed at 6.1 m AGL, sampled every 3 s, with 10 min averages. Wind gusts are defined as the maximum observed wind speed in the preceding hour. The National Oceanic and Atmospheric Administration (NOAA) NWS temperature and humidity are observed at 2 m AGL and winds at 10 m AGL (following the World Meteorological Organization—WMO standards). Data were downloaded from the following website: https://mesowest.utah.edu/.

Station	Location	Latitude (8N)	Longitude (8E)	Elevation (m)	Type
KIZA	Santa Maria Airport (SYV)	34.607	2120.076	205	NWS
LPOC1	Los Prietos (SYV)	34.544	2119.791	299	RAWS
RHWC1	Refugio Hills	34.517	2120.075	447	RAWS
MPWC1	San Marcus Pass	34.491	2119.796	454	RAWS
LRVC1	Lauro Reservoir	34.457	2119.724	204	RAWS
SBVC1	Botanic Garden	34.456	2119.706	230	RAWS
TT367	Powerline-I	34.468	2119.671	656	RAWS
MOIC1	Montecito II	34.445	2119.626	87	RAWS
KSBA	Santa Barbara Airport	34.426	2119.844	3	NWS

with a cutoff low was observed off the coast of Oregon and Washington, while mean sea level pressure gradients intensified around 348N (Fig. 3a), enhancing midto low-tropospheric winds (Figs. 3c,d) over California. This trough slowly moved eastward (Fig. 3b) maintaining westerly winds with speeds of about 15.4ms^{21} at 500-hPa in north of Point Conception (34.458N, 120.478W) on 29 April (Fig. 3d). At lower levels (below 700hPa) and over the ocean next to the SB channel, winds shifted to a northwesterly direction (backing winds) with speeds exceeding 15ms^{21} in the region of interest (Figs. 3e,f).

Wind advisory was issued by the NWS LOX from evening-to-early morning on 27–28 April for SYM southernslopes.Ontheeveningof27April(;2000PDT), the NWS reported 24.5 hPa pressure differences between KSBA and KSMX, suggesting potential conditions for strong gusty winds on the lee of the SYM with prevailing northwest direction, particularly near canyons and passes. On 28 April, pressure differences between these two locations increased to 25.2hPa confirming the expected forecasts. This value is comparable to what was observed during the Jesusita Fire (5–7 May 2009) as both events share similar synoptic conditions (Cannon et al. 2017).

5. Results from SWEX-P

a. Observational analysis

1) SURFACE STATIONS

Local conditions near ground level were evaluated based on the existing network of RAWS and NWS stations (Fig. 1, Table 2). Wind speeds and gusts exhibited large spatial and temporal variability on the lee of the SYM, and in the SYV during SWEX-P (Fig. 4). Differences of wind speed and direction across the SYM and in the SYV demonstrate the importance of the east–west-oriented mountain barrier in enhancing the northerly winds leeward of the SYM. For instance, upstream in the SYV at the KIZA station, which is approximately aligned with RHWC1 on the leeside of SYM (Fig. 1), west (W) and west-northwest (WNW) winds peaked ;10ms^{21} during 1700–1800 PDT (Fig. 4, top row). However, throughout the evening hours, winds were less than 2.5 ms^{21}. Likewise, LPOC1 in the SYV, which is approximately aligned with MPWC1 on the leeside of SYM (Fig. 1), exhibited winds less than 3 m s^{21} throughout the day and particularly in the night, with predominant westerly direction (Fig. 4a) . These nighttime light winds in the SYV indicate a decoupling from the winds aloft associated with nocturnal surface cooling and increased stability.

However, a distinctive scenario in wind speeds and direction was observed leeward of the SYM (Fig. 4,

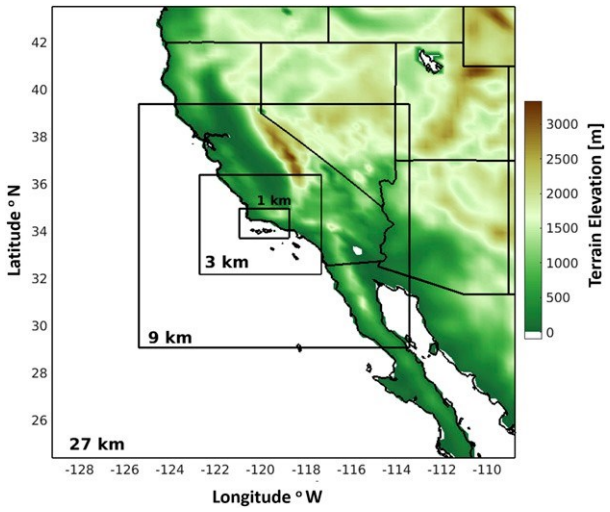

FIG. 2. WRF nested domains and topography (at 27-km resolution); inner domain: 1 km.

TABLE 3. WRF Model configuration settings (Duine et al. 2019).

Model version	WRF, v3.9.1
Simulation start	1100 PDT 27 Apr 2018
Simulation end	1700 PDT 29 Apr 2018
Time step (outermost domain)	120 s
Parent–child ratio	1:3
Nesting	Two-way nested
Grid size innermost domain	1 km 3 1 km
Vertical levels	55 eta
Land cover	USGS
Global input data	ERA-Interim
Microphysics	Thompson (Thompson et al. 2016)
Longwave radiation	RRTMG (Iacono et al. 2008)
Shortwave radiation	RRTMG (Iacono et al. 2008)
Cumulus (27, 9 km)	Modified Tiedtke (Tiedtke 1989; Zhang et al. 2011)
PBL scheme	MYNN 2.5 (Nakanishi and Niino 2006)
Land surface model	Noah with modified z_0 parameter

bottom row). For instance, the westernmost station (RHWC1, elevation 446m) recorded the strongest offshore winds and gusts among all stations, with prevailing north-northwest (NNW) direction during the entire experiment. The peak of these winds (20ms^{21}, ;40kt) and gusts (26ms^{21}, ;50kt) were observed on 28 April, at 2200 PDT. These are considered gale force winds and represent hazardous conditions for aviation. The MPWC1 (elevation 454.5m) showed similar behavior, although with weaker winds. For instance, at 2200 PDT, MPWC1 recorded a mean wind speed of ;13ms^{21} (24kt) with gusts of ;20ms^{21} (;40kt). The wind direction at MPWC1 was predominantly WNW during daytime and shifted to NW and NNW during nighttime, when winds were stronger (Fig. 4). The RHWC1 and MPWC1 stations are approximately at the same elevation (8.5m difference) and the distance between them is roughly 26km, demonstrating the dramatic east–west gradient in wind speed during this Sundowner event, with stronger winds observed downslope of the western (lowest elevation) portion of the SYM. Farther east (;12km from MPWC1 and 38km from RHWC1), despite the relatively higher elevation (652m), the TT367 station recorded maximum sustained wind speed of 9.4ms^{21} (18.0 kt) and gusts of 14.7ms^{21} (29kt) at 2200 PDT. Interestingly,windsweakenedafter2200PDT, but a secondary peak was observed again around 0300 PDT the next morning (;10 m s^{21} with gusts ;13ms^{21}). The reintensification of winds around that time was not observed at RHWC1 and MPWC1 stations, but was a remarkable feature identified with the radiosondes [section 5a(2)]. Also relevant, the southerly winds at TT367 in the afternoon indicated the influence of the onshore marine flow. Wind direction shifts to north after ;1600 PDT until the morning of the next day. Wind characteristics in the westernmost stations on the lee of the SYM suggest that SWEX-P occurred during the ''Gaviota-type'' of event (Gaviota is the westernmost area of the east–west oriented SB coast) discussed in Smith et al. (2018a). While the ''western'' or ''Gaviota'' Sundowner is perhaps the most frequent type of Sundowner event (Smith et al. 2018a), the ''eastern'' regime has been observed during spring and other seasons (Duine et al. 2019; Sukup 2013).

Farther east and on the foothills of the SYM, the LRVC1 station (203.9m) recorded maximum wind speeds (;13.0ms^{21}, 25kt) and gusts (;15ms^{21}, 29kt) with direction varying from WNW to NNW between 1600 and 2100 PDT. The SBVC1 station (229.5m), which is located approximately 1.6km east of LRVC1, recorded relatively stronger winds, despite their proximity and similar elevation. RAWS stations are usually placed in locations that are fire prone and differences in terrain and land cover can contribute to local variations in winds. A peak in wind and gusts (;30kt) with dominant NNW direction was observed at SBVC1 between 2100 and 2300 PDT, indicating a delay in the onset of gusty winds with respect to the LRVC1 station.

The easternmost station (MOIC1), located on the foothills of the SYM (elevation 86.9m) and approximately 7.5km east of SBVC1, showed a shorter influence of Sundowners comparatively to other stations. Southerly winds less than 3ms^{21} dominated from the morning to the afternoon of 28 April, indicating the influence of the onshore (sea breeze) circulation. Sundowners with dominant north-northeast (NNE) direction initiated between 2000 and 2200 PDT, much later than at other stations.

The KSBA station (3m) diurnal cycle of winds direction in three distinct pulses at 2100 PDT 28 April, 0100

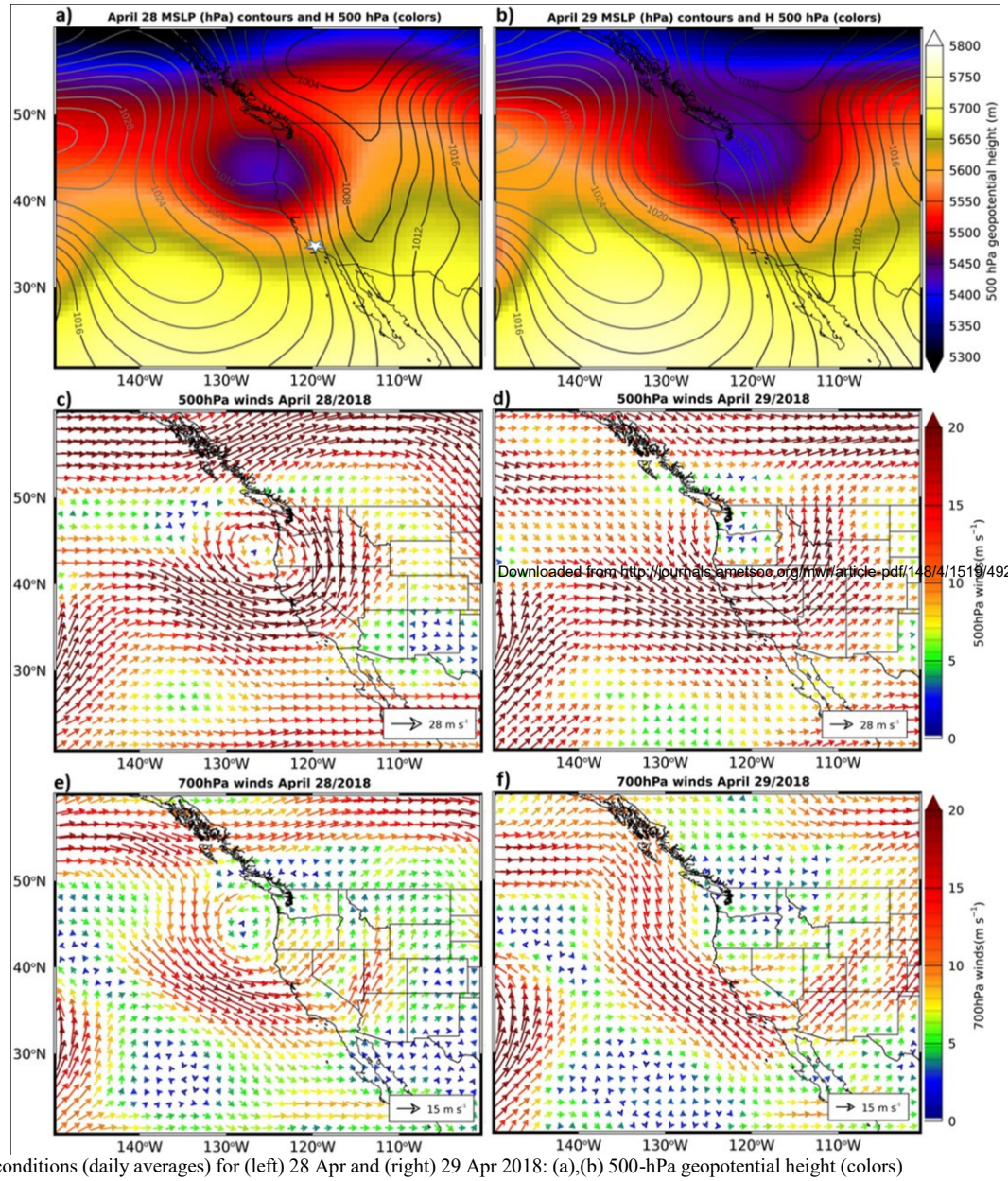

FIG. 3. ERA-Interim synoptic conditions (daily averages) for (left) 28 Apr and (right) 29 Apr 2018: (a),(b) 500-hPa geopotential height (colors) and sea level pressure (contours); (c),(d) 500-hPa winds; (e),(f) 700-hPa winds. White ''star'' symbol in (a) indicates the approximate geographic location of Santa Barbara.

significantly differed from other stations during SWEX-P. In fact, KSBA's relative proximity to the ocean renders this station a unique local climate that is mostly influenced by the strength of the MBL and is often decoupled from the local climate represented by stations on the foothills and slopes of the SYM (Cannon et al. 2017; Duine et al. 2019). During SWEX-P, we observed the peak of winds at KSBA during midafternoon (between 1300 and 1700 PDT), when wind speeds reached ;10 m s^{21} with dominant W direction. Winds weakened after 1700 PDT but reintensified with northerly and 0300 PDT 29 April (Fig. 4). As discussed in the next section, these northerly winds seemed consistent with the observed behavior of the nocturnal lee jet identified with radiosondes.

Another noticeable aspect was the difference in the onset of Sundowners in stations located in the foothills and slopes of the SYM: the earliest (latest) onsets of the NNW (NNE) winds were generally observed at the westernmost (easternmost) stations (Fig. 4, bottom row). The eastward lag in the onset of Sundowners and differences in wind direction

between eastern and western parts of the SYM have been noticed before by NWS LOX forecasters and in Sukup (2013), and in model simulations (Smith et al. 2018a).

The adiabatic warming accompanying these downslope winds may vary in intensity and vertical extent depending on multiple factors, including the characteristics of the mixed layer over the Santa Ynez valley, mountain slopes and coast, and topographic elevation. Local variations in temperature may depend on a combination of effects, including diabatic heating and cooling rates, temperature advection by the winds (Turton et al. 2017) and turbulent mixing (Whiteman 2000). For Sundowners, some of these effects are strongly linked to the synoptic forcing that are seasonally dependent (Blier 1998). Moreover, the SYM varies in elevation: the lowest (highest) mean altitudes ;670 m (;1200 m) are observed west (east) near Gaviota (Montecito) (Fig. 1). Thus, warming resulting from adiabatic compression may be difficult to separate from other effects based on ground observations. Accordingly, stations on the southern slopes of the SYM showed very subtle changes in the cooling rate during evening hours associated with the peak of Sundowners during SWEX-P (Figs. 5a,c). For most stations, temperatures remained approximately constant (KSBA, SBVC1, TT367) and only a few stations showed less than 38C increase in temperature between 2000–2200 PDT 28 April (SBVC1, TT367) and 0100–0200 PDT 29 April (MOIC1). However, some stations reported significant decrease in relative humidity (Figs. 5b,d) (LRVC1, SBVC1, MOIC1, TT367) during the peak of the winds. The drop in relative humidity combined with strong winds is relevant during wildfires. The presence of a ''thermal belt'' at high elevations of the SYM contrasting with the cold and humid marine layer at lower elevations has been reported by fire fighters during Sundowners (Chief R. Hazard 2018, personal communication).

Although RHWC1 showed the strongest winds among all stations, temperatures decreased at a steady rate during the evening hours indicating no relevant net adiabatic warming effect. This is not surprising considering the relatively low elevation of the western SYM (;650 m), and the fact that RHWC1 is near the mountain ridge and more influenced by the MBL and coastal jet (Rahn et al. 2014). Therefore, this study did not support the results shownin Smith et al. (2018b) regarding the ''ramp in temperature'' observed during the Sherpa Fire (June 2016), suggesting that this criterion should not be generalized as a metric toevaluate Sundowner winds at all locations and elevations leeward of the SYM. More studies and additional observations in distinct seasons are necessary to properly evaluate the Sundowner warming effect on the southern slopes of the SYM.

It is worth noticing that both stations in the SYV (KIZA and LPOC1, Figs. 5e,f) exhibited a diurnal cycle in temperatures much more coherent with the western stations RHWC1andMPWC,withmaximumtemperaturearound 1300 PDT and minimum before sunrise (LPOC1). They also show much less variability in temperature (Fig. 5e) and relative humidity (Fig. 5f) during the night comparatively with stations downstream of the SYM.

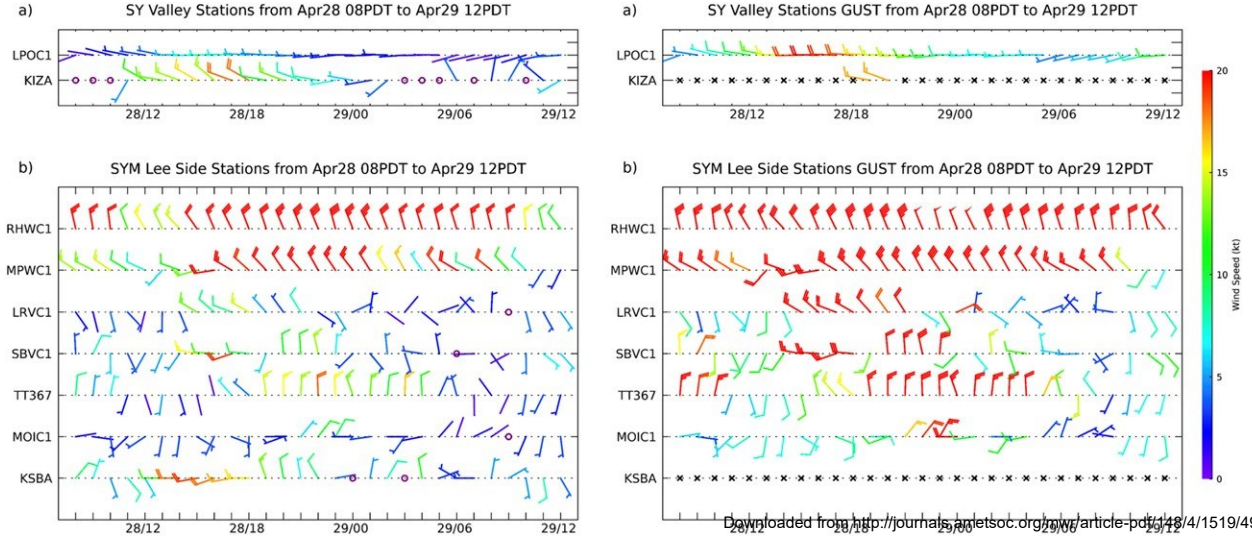

FIG. 4. (left) Wind speed and direction and (right) wind gusts and direction observed in surface stations during SWEX-P. Station acronyms in vertical axes correspond to stations shown in Fig. 1. Horizontal axes show day and local time. Colors represent wind intensity (units: kt).Stations at the top roware locatedin the SantaYnezValley(LPC1,KIZA). Otherstationsare locatedleewardof theSYM. The ''3'' symbol indicates no observation and ''s'' indicates calm winds. Notice that RAWS stations do not report wind gust direction. For the sake of this plot, gusts direction is assumed to be the same as the direction of the mean winds.

2) RADIOSONDE DATA

SWEX-P provided a unique opportunity to evaluate vertical profiles of winds along with parameters of stability in the environment representative of atmospheric conditions leeward of the SYM that are conducive to Sundowners. To understand these environmental conditions, we begin by analyzing profiles of wind speed and direction, virtual potential temperature (u_y), mixing ratio (q), and stability parameters from the boundary layer to the midtroposphere, preceding, during and after the peak of Sundowners on the evening of 28/29 April (Fig. 6). Skew T–logp plots of individual radiosonde profiles are also shown in the supplemental material (Fig. S1 in the online supplemental material).

(i) The morning of 28 April 2018

The morning radiosonde (0800 PDT) on 28 April, launched after sunrise (sunrise in SB is 0612 PDT 28 April), showed a stratified atmosphere at low levels with cool temperatures (14.38C) and high relative humidity (76%) near ground level, capped by a shallow inversion between ;100–150m AGL (not shown). Calm winds (less than $1ms^{21}$) with SE direction near ground level (below 500m AGL) indicated the presence of the onshore marine flow (Figs. 6a–c). However, above 500m AGL, wind speed intensified and changed to NW direction with peak intensity (;$7.4ms^{21}$) between 900 and 1100m AGL (Figs. 6b,c). As the atmosphere over land warmed, onshore winds [southeast (SE)–southwest (SW) direction] intensified over a narrow layer capped by a stable layer of increased moisture near the surface (Figs. 6a,b). The profiles of q (Fig. 6a) and u_y (Fig. 6b) indicated the presence of a shallow mixed layer and a residual layer directly above. Winds intensified backing with

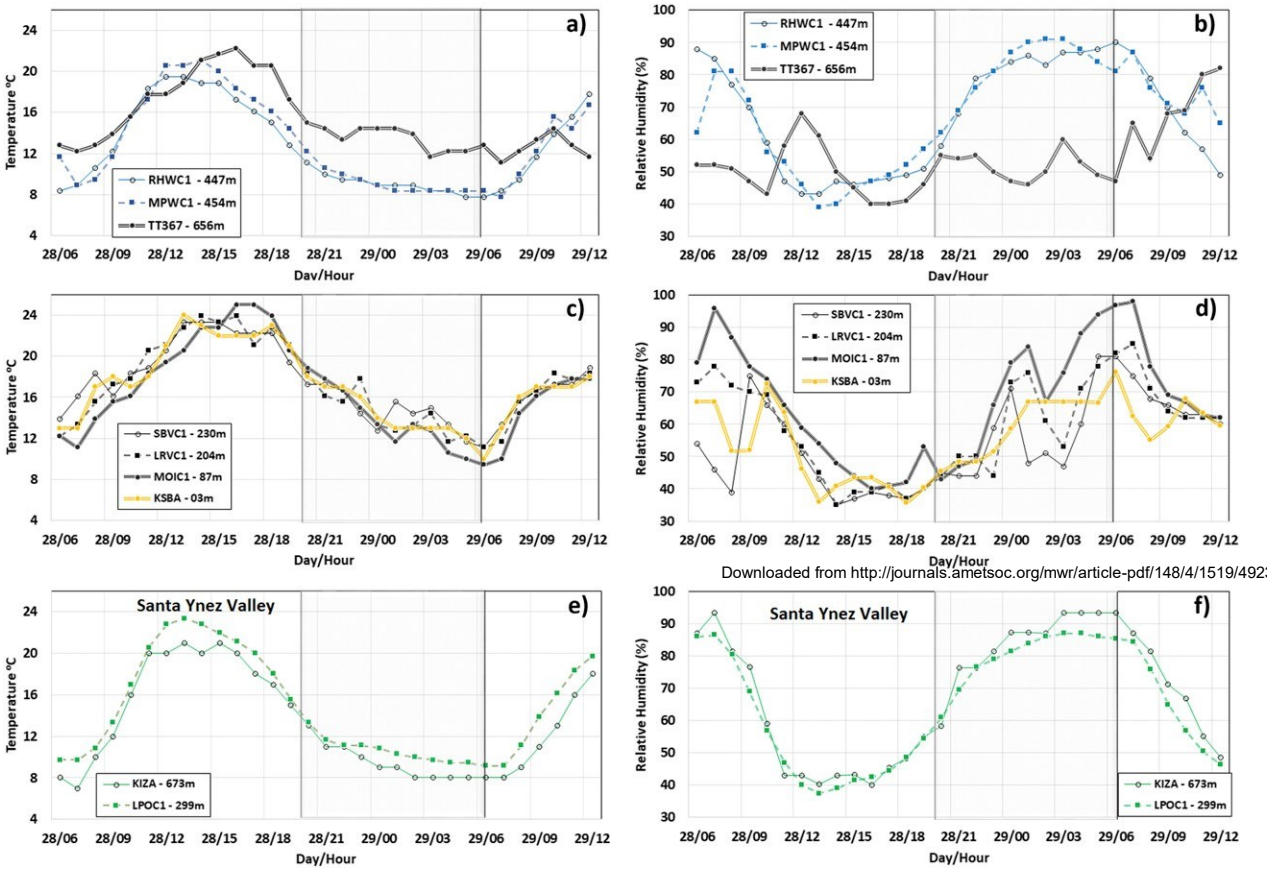

FIG. 5. (a),(c),(e) Temperature and (b),(d),(f) relative Humidity temporal evolution observed in surface stations: (top) southern slopes of the SYM above 400 m; (middle) southern slopes of the SYM below 250 m (KSBA station near the coast is indicated in yellow); (bottom) Santa Ynez Valley. Horizontal axes show day and hour (PDT). Light gray shading indicates hours between sunset and sunrise (PDT). Stations located in the western portion of the SYM are shown with blue color in (a),(b); all other stations located in the middle and eastern portion of the southern slopes of the SYM are indicated with back color. Stations in the SYV are in green in (e),(f). Geographic location of these stations are shown in Fig. 1.

elevation (Fig. 6b), reaching 10ms^{21} (25 mph) at ;1500m AGL with NW direction (Fig. 6c).

(ii) The afternoon of 28 April 2018

At 1400 PDT the profile of u_y indicated the presence of a superadiabatic layer below 500m AGL and a deeper mixed layer above extending up to ;1200m AGL (Fig. S1). Westerly winds intensified near ground level, backing with elevation (Fig. 6b). The increase in mixing ratio (;10gkg^{21}) near ground level indicated moisture advection from the ocean, characterizing the presence of a shallow MBL. Similarly to the previous sounding, wind speed intensified with elevation and variations in wind speed indicated that turbulent processes (dynamic and convective) were important in determining the profile of winds below 1000m AGL.

At 1700 PDT, a dramatic change in winds, temperature and stability profiles below 1000m AGL was observed. Convective instability decreases near ground level and a shallow mixed layer formed (;150–300m AGL) capped by an inversion layer (;300–900m AGL) (Fig. 6a). Simultaneously, we observe that the 300-K isentrope was transported downward from ;1900m to ;750m (Fig. 6b). The downward transport of upper air in the lee of a mountain range is a remarkable feature of downslope windstorms (Durran 2003; Grubisic´ and Billings 2007; Cannon et al. 2017). Below this inversion, wind speeds intensified, characterizing an abrupt onset of a low-level jet with peak in wind speed of ;12.0ms^{21} and WNW direction at 490m AGL. The intensification of the winds and gusts at some of the eastern stations closer to the launching (MPWC1, LRVC1, and SBVC1, Fig. 4) was

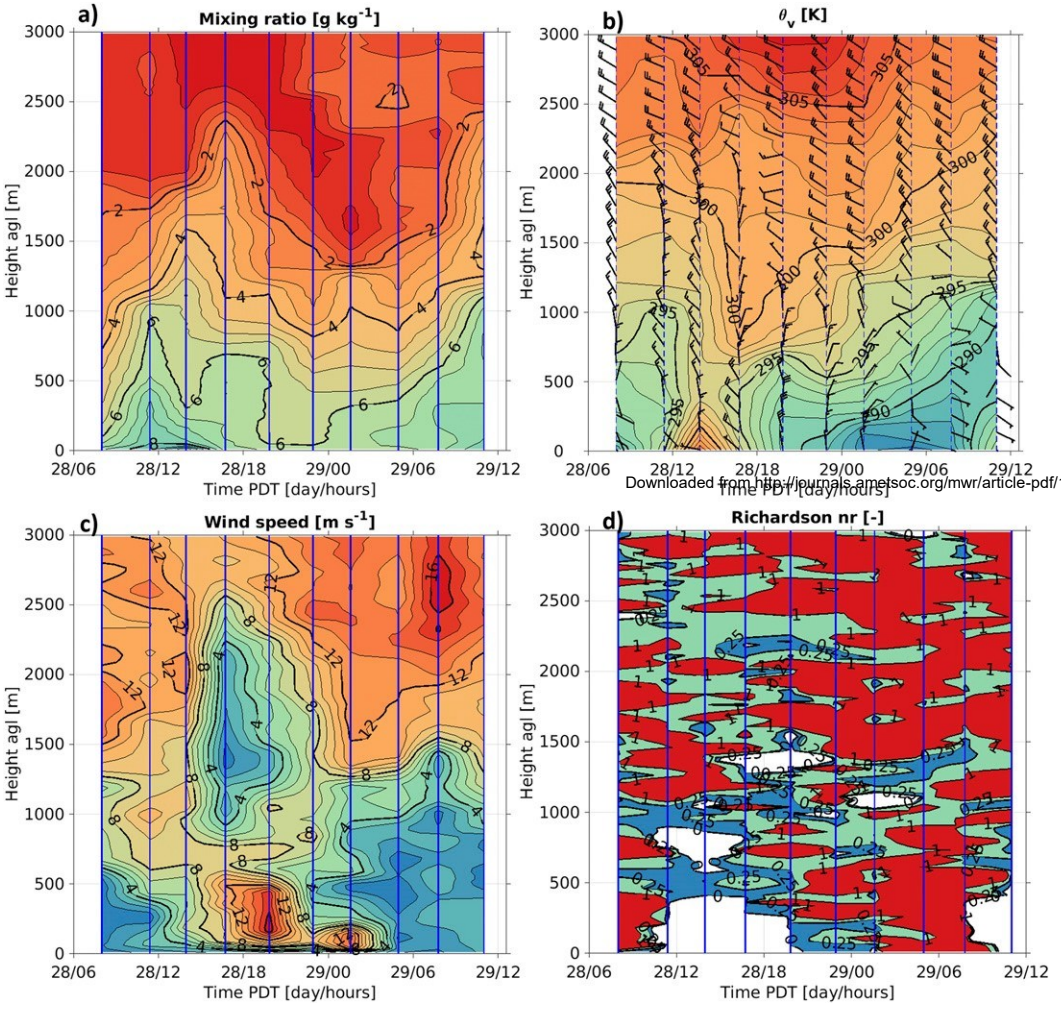

FIG. 6. Radiosonde profiles of (a) water vapor mixing ratio (g kg^{21}); (b) virtual potential temperature (K), wind speed (kt), and direction (conventional); (c) wind speed (m s^{21}); and (d) bulk Richardson number R_B (blue color indicates R_B# 0.25 and green color 0.25 , R_B# 1.0). Radiosonde data were interpolated to provide a continuous evolution of the variables during SWEX-P. Vertical thin lines show time of radiosonde launches. Hours are PDT.

consistent with these features. At 1700 PDT, the elevation of

the sun was approximately 328 (at sea level), whereas the azimuthal angle was 2648; therefore, less direct sunlight was available at the southern slopes of the mountains. The decrease in solar radiation may explain the rapid variation in the profiles of temperature (Figs. 6a and 5a,c), stability (Fig. 6b) and winds (Figs. 6c and 5) detected by radiosondes and stations.

(iii) The evening of 28–29 April 2018

The most remarkable characteristic of Sundowners is the peak in wind speeds and gusts from early evening through early morning. The astronomic sunset on 28 April was at 1940 PDT. The 1950 PDT radiosonde was launched right after the sunset. The southern facing slopes of the SYM were already in the shade before sunset and cooled fast after sunset. The surface cooling enhanced stability in the boundary layer adjacent to the slopes creating environmental conditions conducive to the development of a nocturnal lee jet (Stull 1988). Upwind in the SYV, winds were calm and temperatures begin to decrease abruptly after 1700 PDT (Fig. 5), earlier than most stations on the slopes of the SYM east of Refugio (Fig. 1). This suggests that the convective mixed layer upstream in the SYV may have already collapsed around the time of the onset of Sundowners. During strong synoptic forcing (strong pressure gradients) and increased stability near crest level, farther
downslope acceleration may occur as predicted by the hydraulic analog theory (Durran 2003). The 2000 PDT radiosonde showed a well-defined northerly jet and maximum wind speed of ;17ms^{21} at 168m AGL
(Figs. 6b,c). Above this level, winds were relatively calm (;2ms^{21} at about 1420m AGL). The strong shear created by the lee jet was accompanied by changes in wind direction, with northerly winds observed at lower levels. These winds were directed across the isobars (not shown), consistent with the rule of thumb adopted by the NWS LOX to predict Sundowners. Additionally, the remarkable wind shear caused turbulence and enhanced gustiness in all stations (Fig. 4).

To evaluate the mechanical production of turbulent kinetic energy (TKE) using radiosondes, we calculated the bulk Richardson number:

$$R^B = \frac{g D\theta\, Dz}{\overline{u_y}\left[(D\overline{U}^2)1_y(D\overline{V}^2)\right]}, \qquad (1)$$

where g is gravity (ms^{22}), DU/Dz, DV/Dz, and Du_y/Dz are approximate vertical gradients (over increments of 25m) of zonal and meridional winds and u_y, respectively, obtained from radiosondes (Stull 1988). The R_B provides a good estimate of the balance between mechanical production of TKE [denominator of Eq. (1)] and buoyancy consumption [numerator of Eq. (1)]. At 2000 PDT, stability identified by the Brunt–Väisälä frequency $N = [(g/u_y)(Du_y/Dz)]^{1/2}$ increased between 500 and 1000m AGL, just above the jet. The strengthening of the jet increased mechanical turbulence that could not be balanced by the buoyancy consumption of TKE, decreasing R_B to values less than 0.5. These results suggest that the environment below 500m was approaching the critical theoretical Richardson number $R_c = 0.25$, for which the laminar flow becomes turbulent (Fig. 6d). The increase in turbulence explains the enhancement in wind gusts observed at ground level in most stations around this time (Fig. 4).

However, turbulence is dissipative. With no further sources of TKE, increasing mechanical turbulence may lead to a decrease in wind speed at the jet level by mixing air with lower momentum near ground level. In fact, the radiosonde at 2300 PDT detected a decrease in the strength of the jet from 17ms^{21} at 2000 PDT to 9.5ms^{21} at 2300 PDT (Fig. 6c). Wind speeds and gusts decreased around 2300 PDT in most stations (Fig. 4, bottom row) providing further evidence of the importance of dissipation caused by turbulence.

Conversely, the decrease in wind speed may have enhanced the rate of nocturnal radiative cooling near ground level, which can also be noticed from temperatures in all stations (Figs. 5a,c). The enhanced cooling at ground level increased stability (Du_y/Dz) and therefore N^2 near the slopes of the SYM. The 0200 PDT radiosonde on 29 April showed a remarkable strengthening of the nocturnal lee jet (maximum speed 14ms^{21}) with northerly direction at its lowest elevation (45m AGL) during the evening. This remarkable intensification of the jet (which was a noticeable feature at the radiosonde site located at 84m msl) at very low elevation was accompanied by rapid cooling (Fig. 6b) near ground level. Although the cooling suggests the influence of slope (katabatic) flow (Grachev et al. 2016), wind speeds seemed too high for this mechanism to explain the intensification of the jet. Interactions between downslope winds from the San Rafael Mountains are possible mechanisms to explain these winds. More details are discussed in section 5b. The decrease in R_B to values below 0.5 (Fig. 6d) near ground level suggests the enhancement of turbulence consistent with the intensification of winds and gusts recorded in most stations. Conversely, dissipation induced by enhanced me-

chanical turbulence (Fig. 6d) may have influenced the weakening of the flow near ground level in subsequent hours (Fig. 6c).

In fact, the 0500 PDT radiosonde on 29 April, launched approximately one hour before sunrise (0610 PDT), showed a completely different environment. Weak winds (less than 5ms^{21}) were observed from the surface up to ;1000m AGL (Figs. 6b,c) accompanied
by a shallow but pronounced inversion layer in the first 90–100m AGL (Fig. 6b). Consequently, R_B increased to values greater than 1 (Fig. 6d) and these conditions were sufficient to dissipate the jet (see supplemental Fig. S1 for details). At this time surface stations detected the weakest wind speeds and gusts during the evening (Fig. 4).

(iv) Morning of 29 April 2018

The 0800 and 1100 PDT radiosondes showed a stratified atmosphere below 2500m AGL and increased relative humidity and mixing ratio from ground level to about 250m AGL (Figs. 6 a,b). Winds were calm (wind speeds were ,5ms^{21} below 1500m AGL) (Fig. 6c) with dominant ESE direction near the surface indicating the influence of the MBL (Fig. 6b).

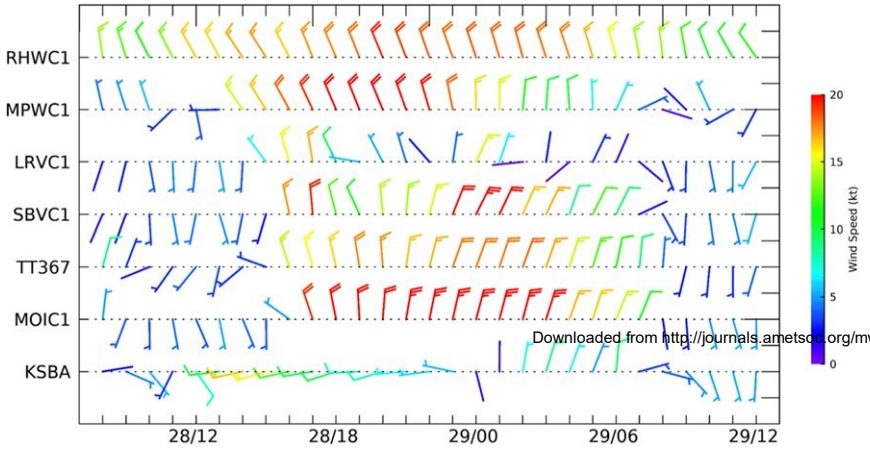

FIG. 7. WRF (1-km resolution) simulation of winds (kt) for stations at the lee of the SYM (Fig. 1). Station names are shown in Table 2.

b. Mesoscale simulations with WRF

1) COMPARISON WITH SURFACE STATIONS

Simulated winds at the station locations in the lee of the SYM are shown in Fig. 7. Despite the wind-height correction, WRF overestimated wind speeds at some sites and underestimated in others when compared to stations (cf. Fig. 7 with Fig. 4). This behavior is rather common and depends on many factors including anemometer exposure and grid cell representation in complex terrains (Cao and Fovell 2016, 2018; Duine et al. 2019). At RHWC1, WRF greatly underestimated wind speed but showed very good skill in simulating wind direction. Interestingly, WRF showed a better skill in simulating the observed winds near MPWC1, capturing the increase in wind speeds in the afternoon and peak around 1900 PDT, although underestimating the two peaks in the evening associated with the strengthening of the nocturnal lee jet.

Nonetheless, at LRVC1, the transition between onshore and offshore winds and the intensity of the winds were remarkably well captured. At SBVC1, WRF had problems in properly simulating the daytime onshore flow and onset of Sundowners, and overestimated wind speeds at night, with simulated speeds more consistent with the observed wind gusts. Moreover, the simulated wind direction at MOIC1 shared similarities with SBVC1, whereas observations showed great differences, particularly during daytime. Notice that observations may have been influenced by local surroundings, while the model at 1-km grid spacing resolved a slope with similar gradients and orientations at both locations. WRF showed a shift in wind direction (from onshore to offshore) and increase in wind speed much earlier in the simulations than in observations.

Simulated winds at KSBA showed a late onset of the northerly winds compared to other locations closer to the foothills of the SYM. KSBA is strongly influenced by the MBL (Duine et al. 2019). The chosen configuration maintained westerly winds at that site until about 0100PDT, while observations indicated that KSBA was affected by northerly winds around sunset. However, both model and observations show consistent weak northerly winds at the location after this period, in agreement with the secondary peak in the jet [see sections 5b(4) and 5b(5)].

2) SEA LEVEL PRESSURE DIFFERENCES

The NWS LOX relies on the magnitude of MSLP differences between two pairs of stations (KSBA and KSMA, and between KSBA and KBFL) for their forecast of Sundowner winds and to issue fire-weather alerts. Observations and WRF simulations of MSLP differences between these locations are shown in Fig. 8. Observations indicated the most significant differences between KSBA and KSMA (Fig. 8b), with differences reaching 25hPa after sunset (;2100 PDT) on 28 April. However, MSLP differences decreased in subsequent hours, while the nocturnal lee jet remained intense and gusting at ground level. Thus, the MSLP difference criteria, although important in forecasting the potential for significant Sundowners to occur, was not sufficient to predict the observed nighttime behavior of winds on mesoscale. Differences between KSBA and KBFL (Fig. 8a) were negative but relatively less significant (#3.0 hPa in magnitude) consistent with the ''Gaviota-type'' of Sundowners discussed in Sukup (2013) and Smith et al. (2018a) and investigated here. WRF simulated well the observed trends in MSLP differences during the period of the experiment. The timing of maximum MSLP difference between KSBA and KSMA was simulated approximately between 1800 and 2000 PDT, consistent with the onset of the nocturnal lee jet in the model.

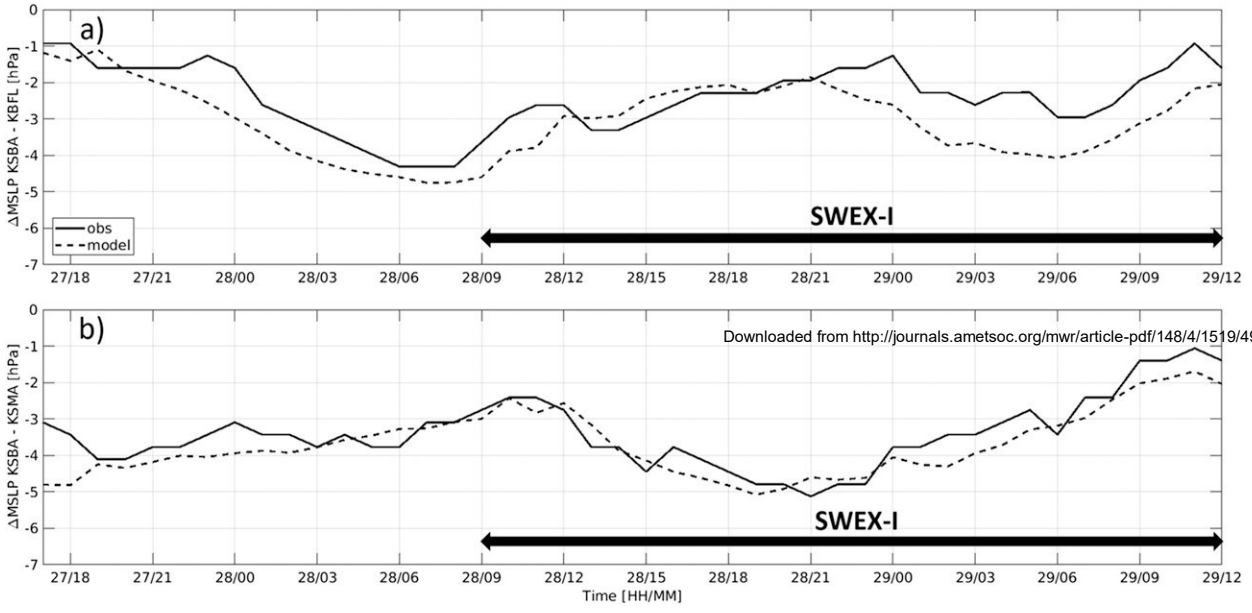

FIG. 8. WRF simulated (dashed lines) and observed (solid lines) differences in mean sea level pressure (DMSLP) between: (a) Santa Barbara airport station (KSBA) and Bakersfield airport station (KBFL); and (b) Santa Barbara airport station (KSBA) and Santa Maria airport station (KSMA). Sign convention adopted in these plots is the same as used by the NWS LOX.

3) VERTICAL PROFILES AT THE SWEX-P LAUNCH SITE

Simulations of vertical profiles were evaluated at the nearest grid point to the launching site (model elevation 88m, actual elevation 84m). A detailed comparison between all radiosonde profiles of temperature, dewpoint and winds and WRF simulations of the same variables can be assessed in the supplemental Fig. S1. In agreement with observed profiles, the simulated vertical profiles at the SWEX-P site show a shallow layer with relatively high mixing ratio (Fig. 9a) and weak southerly winds (Figs. 9b,c) in the morning, indicating that the model was able to capture the development of the MBL. A mixed layer gradually developed after 0900 PDT, and increased in both depth and temperature until around 1400 PDT (Fig. 9b), when it reached maximum depth (;2000m AGL).

WRF simulated the intensification of winds below 500mAGLtovaluesexceeding20ms^{21} after;1700PDT (Figs. 9b,c). Notice that wind speeds within the boundary layer are generally higher in WRF than in observations. In late afternoon, a strong stable layer developed in the model at 500m AGL with a vertical u_y gradient of 10Kkm^{21} (Fig. 9b). Between 1500 and 1700 PDT the 300-K isentrope was transported downward from ;2.0km to ;600m, while the 302–305-K isentropes remained close to their elevations. Similar behavior was observed in the radiosondes (Fig. 6b). The downward transport of air masses in the lee of a mountain range is often observed in simulations of downslope windstorms (Vosper 2004), and is considered a crucial

component in the dramatic increase in wind speeds leeward of mountains.

Simulations show the development of the lee slope jet late in the afternoon, with the most pronounced peak in wind speed (;18.0 m s^{21}) around 1900 PDT. An important aspect during development of the lee slope jet in the model (approximately between 1700 and 2100 PDT) was the calm winds above the SYM crest level (i.e., between 1000 and 2000 m, Fig. 9c). This indicates that the model was capable of characterizing the layer where wave breaking occurred and, thus, the potential for downslope windstorm on the lee of the SYM. In the wave-breaking region, WRF simulated R_B less than ;0.25 (Fig. 9d), somewhat consistent with radiosondes that indicated that R_B dropped below 0.5 (Fig. 6d). Simulations show stronger winds at the jet core and a much drier marine layer during daytime (cf. isopleths of 4 and 6 g kg^{21}, Figs. 6a and 9a) and especially during nighttime, comparatively to observations.

During the evening (from 2100 to 2400 PDT), WRF simulated a progressive decrease in strength and upward extent of strong winds associated with the lee slope jet (cf. the 12ms^{21} isotach), as the strong low-level jet mixed in air from layers aloft, reducing the local stability as revealed by the profiles of u_y and R_B (Figs. 9b,d). Wind direction at the surface remained northerly during this period, with a slight preference for northnortheasterly direction aloft (Fig. 9b).

Winds significantly weakened in the simulations around 0000 PDT. Between 0200 and 0400 PDT, a stable layer formed and intensified. Observations (Fig. 6c) indicated that a secondary peak in the jet was observed between 0200 and 0300 PDT 29 April while the model indicates a much weaker lee slope flow with peak wind speedofabout6ms^{21} around0400PDT.After0500PDT, simulations show the onset of the onshore marine flow (southeasterly wind direction and along with higher humidity) below 500m AGL, consistent with observations (Figs. 9a,b).

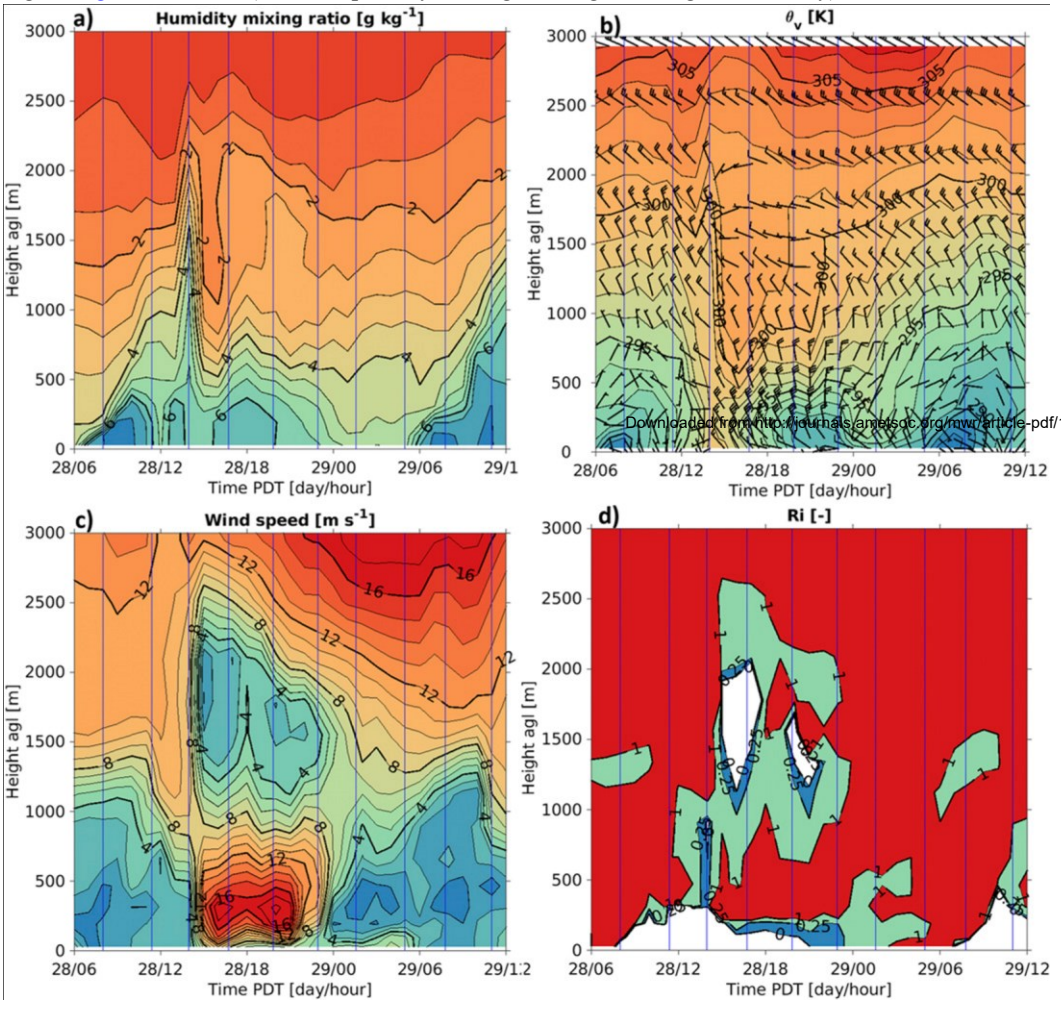

FIG. 9. WRF simulation of the evolution of vertical profiles (same as in Fig. 6).

4) MESOSCALE CHARACTERISTICS OF SURFACE WINDS

The objective of this discussion is to show the spatial variability of the 10m winds based on simulations. At 1400 PDT, strong northwesterly winds are evident in the western portion of the southern slopes of the SYM near Refugio and Gaviota (Fig. 10), whereas westerly winds dominated near the coast, consistent with observations (Fig. 4). In the SYV, we observe relatively weaker winds with WNW direction. Large east–west variations in wind speed are noticeable in the simulations at the lee of the SYM, with the strongest winds (.16ms^{21}) observed over the western slopes of the SYM. Close to the coast, where the KSBA airport is located, WRF shows westerly winds, in agreement with observations (Fig. 4).

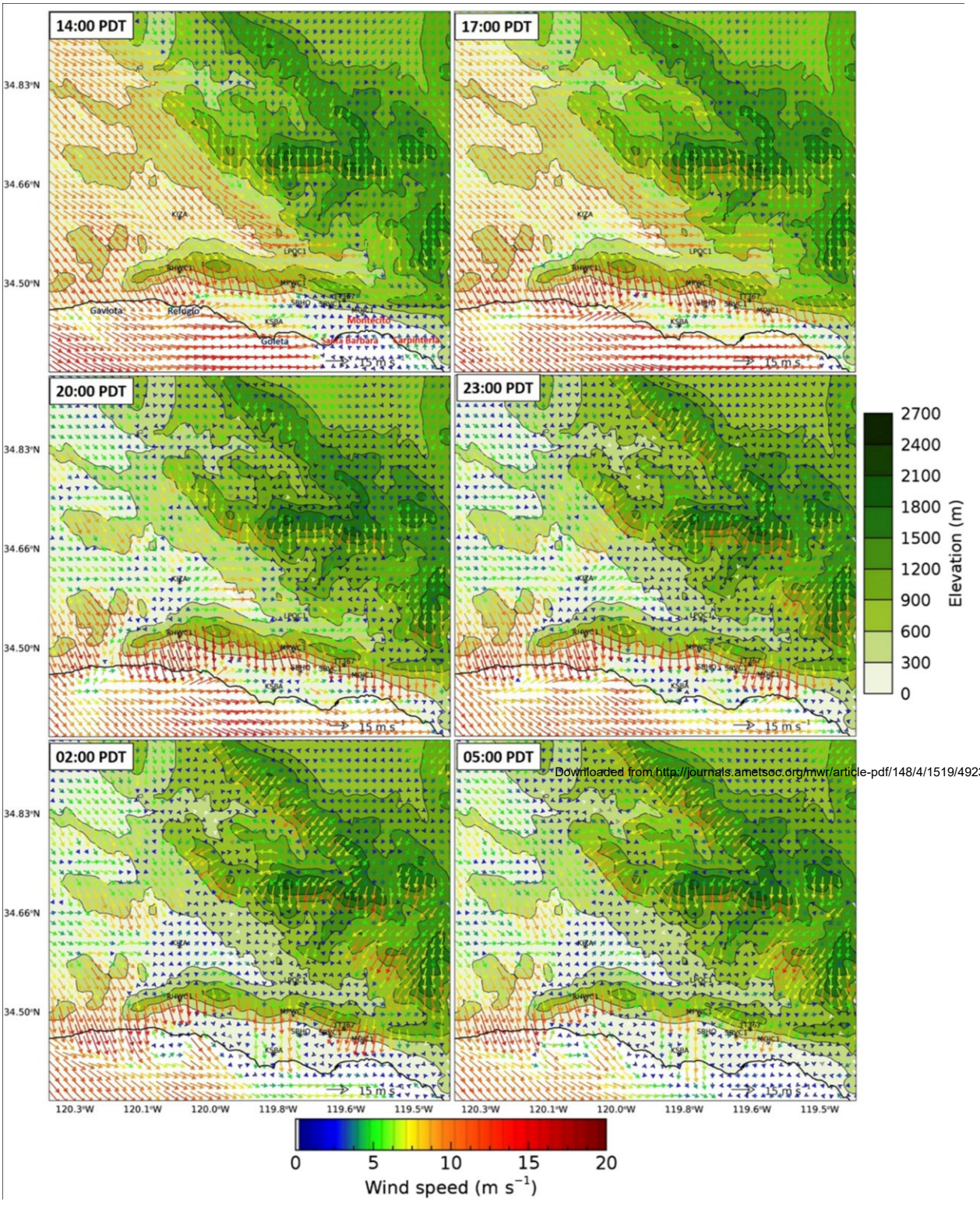

FIG. 10. WRF simulation of 10 m winds (arrows). Time (PDT) is indicated at the top of each frame. The location of the RAWS and NWS stations are indicated as in Fig. 1. Coastal urban areas and landmarks are shown in the first frame for reference.

At 1700 PDT, simulations show the strengthening of wind speeds in the foothills of the entire SYM range, reflecting the observed progressive west–east onset of the strong winds (cf. with Figs. 4 and 7). At 2000 PDT, WRF shows the weakening of winds in the SYV associated with the onset of nocturnal surface cooling and decoupling of the winds aloft. On the southern slopes of the SYM, WRF reveals a completely different pattern: strengthening of 10m winds and shifting to northerly direction. This is the period with the strongest winds on the slopes and foothills of the SYM, with speeds exceeding $18ms^{21}$ in the southern portion of the SYM.

Strong winds on the leeside of SYM were still present in the 2300 PDT simulation but now exhibiting large spatial variability, in agreement with the observations. Near coastal areas and close to the ocean, winds were much weaker compared to the slopes and foothills of the SYM. Additionally, simulations indicated the onset of the NE winds in the eastern SYM whereas NNW (and generally stronger) winds dominated the western slopes of the SYM. Northerly winds were simulated at the center (roughly near MPWC1) indicating the transition between the two regimes. Notice that the onset of the NE winds in eastern SYM seems to coincide with the onset of strong NE winds at high elevations and on the slopes of the San Rafael Mountains.

At 0200 PDT, WRF simulated the strongest winds in the lee of the SYM mostly confined to the foothills. East of the SYM range, strong winds persisted, while winds weakened in the western SYM range, consistent with observations at RHWC1. WRF indicated the presence of gap flows in the western, center and eastern portions of the SYM slopes. These flows may create horizontal wind shear that can induce mesoscale cyclonic eddies in the Santa Barbara channel late in the evening, as suggested by the pattern of winds in coastal areas (Fig. 10). This mechanism may increase the transport cool and stratified MBL air onshore, responsible for the lifting the lee jet, and can be important in explaining the variability of winds, temperature and turbulence along the coast. Notice that the radiosonde indicated a reintensification of the jet at very low elevations at the SWEX-P site around 0200 PDT (Fig. 6c). WRF did not correctly simulate the intensification of the jet at the site, but indicated a relatively strong ($9–10ms^{21}$) gap flow west of the region, where elevation decreases (near San Marcus pass, see MPWC1 station for reference).

At 0500 PDT, simulations showed the weakening of winds throughout the foothills, but still maintaining strong winds on the eastern slopes of SYM, San Rafael Mountains and gap flows. These northerly winds were observed (and simulated) at the KSBA site (Figs. 4 and 7). Also relevant, simulated winds on the slopes of SYM at 0800 PDT also dropped to speeds below $5ms^{21}$ (not shown). Overall, the 24-h simulations showed spatial patterns and temporal variations of winds that were highly consistent with observations near ground level.

To examine the origin of the air mass at the SWEX-P radiosonde site and to contrast the influence of mountain flows and the marine boundary layer on parcel's properties, back-trajectory of the air parcels were investigated using the Hybrid Single-Particle Lagrangian Integrated Trajectory model (HYSPLIT) developed by NOAA's Air Resources Laboratory (Stein et al. 2015; Draxler 1999). Back trajectories calculated with HYSPLIT using WRF simulations are shown in Fig. 11. Trajectories start at 10m AGL at the radiosonde site (SBHQ, Fig. 1). The time indicated in Fig. 11a is when the backward trajectory starts, and the maximum time allowed for these trajectories was 12h. Therefore, the back trajectory ends either when the parcel is outside of the WRF inner domain (Fig. 2) or after 12h. HYSPLIT back trajectories reinforce two important hypotheses in this study: in the morning and afternoon hours, the air mass that reached the SBHQ had strong marine influence. This is indicated by the high pressure (lower elevation) of the back trajectories during the 12h prior they reach the site at1100 and 1400 PDT 28 April (Fig. 11a) and respective nearshore trajectories (Fig. 11b). Conversely, in late afternoon, at 1700 PDT we observe a complete transition from the moist, marine in origin, air mass to a much drier air mass, originated in higher elevationsoftheatmosphere,atpressureslowerthan750hPa (Fig. 11a) and north of the Santa Ynez Valley (Fig. 11b). During the evening, and between 2000 and 2300 PDT, air parcels at the site appeared to originate much above crest level (Fig. 11a) and upstream, north of the San Rafael massif complex (Fig. 11b). These back trajectories are consistent with Smith et al. (2018a) climatology. Between 0200 and 0500 PDT parcels seem to originate from lower elevations (Fig. 11a) and trajectories shifted eastward comparatively to previous hours, possibly influenced by circulation in the San Rafael Mountains [see section 5b(5)]. As we conjectured before, the end of the Sundowner cycle in the morning of 29 April was characterized by the dominant influence of the marine boundary layer, as indicated by the shallow (Fig. 10a) back trajectories at 0800 and 1100 PDT (Fig. 10b).

5) MOUNTAIN WAVES AND WAVE BREAKING

Durran (1990) suggested that wave-induced critical layers can influence the development of downslope windstorms. Wave-induced critical layers usually appear when vertically propagating waves become statically unstable and break.

This wave-induced critical layer can act as a boundary, reflecting the upward propagating waves back toward the surface in the lee of the mountain range. Observations (Fig. 6) and simulations (Fig. 9) both indicate the development of a wave breaking at the SWEX-P site. To further investigate the relationships between the lee jet and mountain waves we examined north–south vertical cross sections of winds (meridional and vertical components) and isentropes at three locations representative of the western (Refugio, across RHWC1), center (across SWEX-P site) and eastern (Montecito, MOIC1) SYM (Fig. 12). Simulations indicate that mountain waves and the lee jet exhibited distinct characteristics along the SYM. At the western portion of the domain (Figs. 12a–e) the drop of the isentropes indicate that wave breaking appeared leeward of the SYM and maintained stationary. In fact, the wave

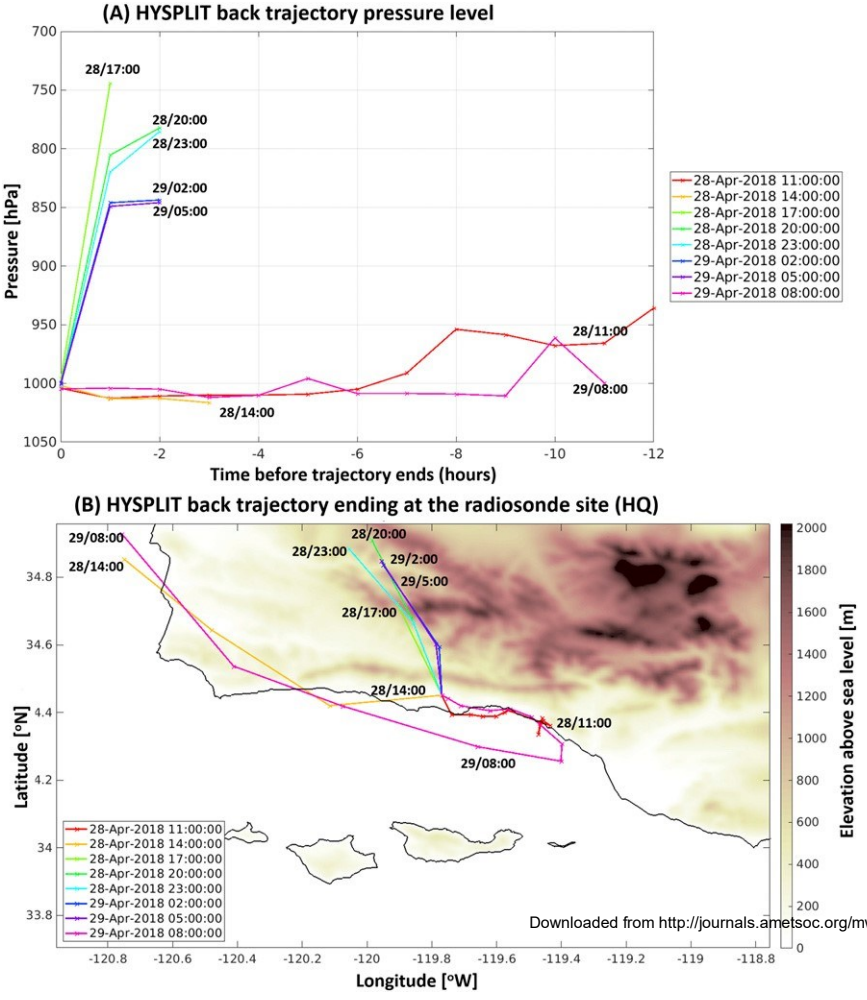

FIG. 11. HYSPLIT back trajectory (12 h) for parcels simulated with WRF at the radiosonde site (SBHQ, Fig. 1): (a) parcel pressure and (b) back trajectory. Time relative to the end of the trajectory is indicated in the figures (day hour[21]) and refers to the time when the parcel reached SBHQ. A trajectory ends when it is outside of the WRF inner domain or after 12 h of duration. The back tracked position of the parcel at every 1-h time interval is indicated by the symbol 3 along each trajectory. Time is PDT.

breaking and a low-level jet were already evident around noon at this longitude (not shown). The characteristics of the jet over the Santa Barbara channel suggest strong association with the offshore low-level coastal jet with northwest direction that has been documented in Dorman and Winant (2000). At the SWEX-P site (SBHQ, Figs. 12f–j), indication of wave breaking in simulations and radiosonde profiles appeared between 1700 and 1900 PDT (Fig. 12f) and seemed crucial to the strengthening of downslope winds leeward of the SYM. WRF simulated this region of wave breaking with R_B values less than 0.25 (Fig. 9d), reinforcing the hypothesis that a wave-induced critical layer had formed above the lee of the SYM at the SWEX site; more importantly, these features were correctly

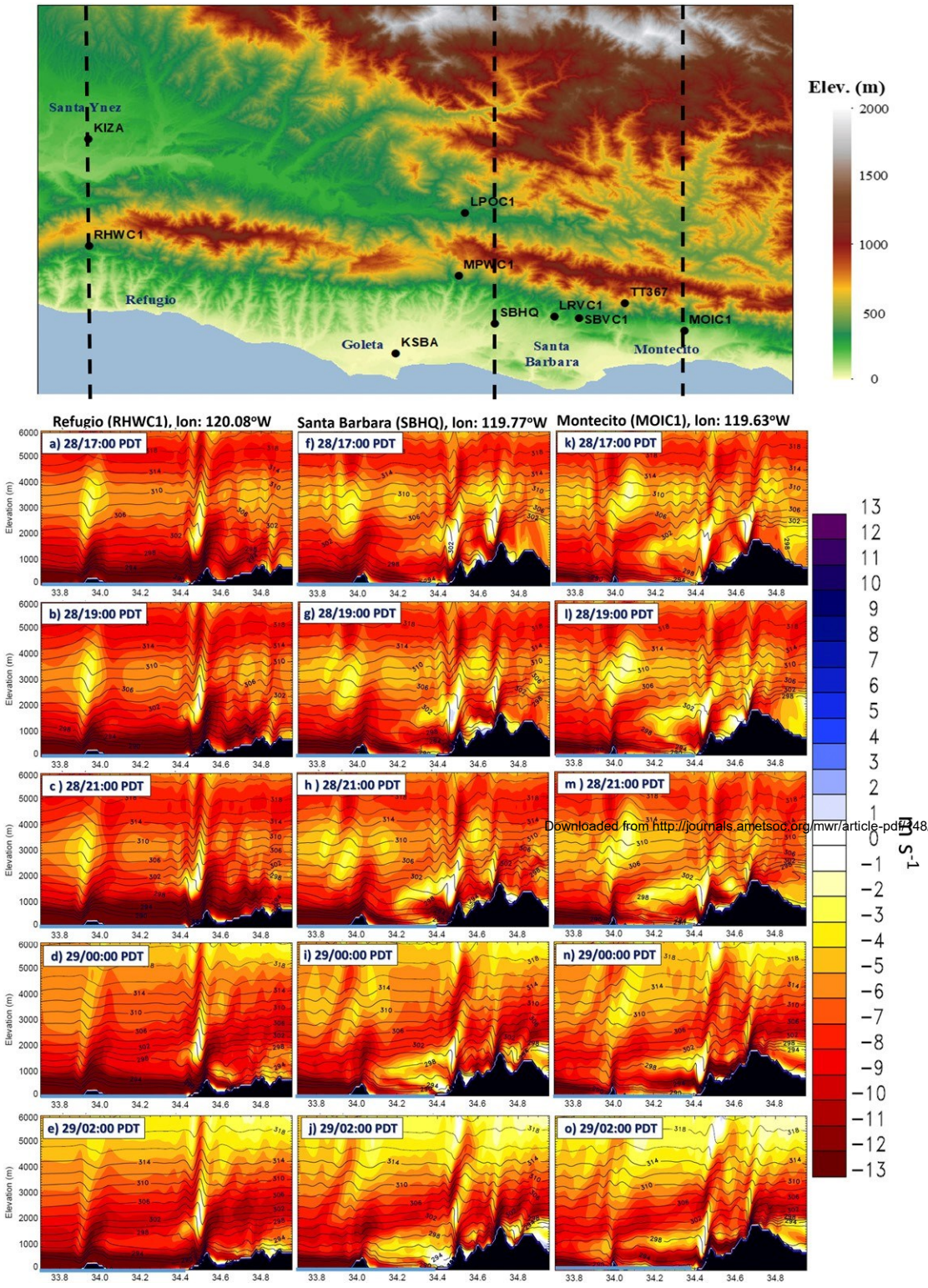

FIG. 12. WRF cross sections (vertical axis shows elevation; horizontal axis shows latitude) at three longitudes indicated in the top map (dashed lines): Refugio (across station RHWC1); SWEX-P site (across station SBHQ); and Montecito (across station MOIC1). Cross sections show cross-mountain meridional wind speed (colors) and theta (contours). Time (hour PDT) is indicated

at the top of each frame. Black shading indicates topography. The relative position of the SYV is shown in the first row for reference. Ocean boundary is shown with a blue thick line.

simulated in a 1-km resolution run using the parameterizations discussed in Duine et al. (2019). It is interesting to notice that the jet is constrained to the mountain slopes where stability increases dramatically, and is much weaker over the channel. Similarly, a lee slope jet appears at the highest southern slopes of the San Rafael Mountains at this longitude. Farther east, across MOIC1 in Montecito (Figs. 12k–o) winds are much weaker leeward of the SYM.

A few hours later (1900 PDT), wind speeds in the lee of the SYM increase for the three longitudes (in simulations and observations) while the wave-breaking region remained roughly stationary until ;2300 PDT, transferring potential energy upstream into kinetic energy, and leading to the dramatic increase of winds on the lee of the SYM (Fig. 12).

After 0000 PDT, winds in the simulations considerably weakened in the foothills of SYM and farther downstream at the coastal plains at the SWEX-P site (Fig. 12h), likely due to the increase in mechanical turbulence (see Fig. 9d). At 0200 PDT the 300-K isentrope retreated upward to about 1800m at the SWEX location (Figs. 9b and 12j), which is in line with observations (cf. Fig. 6b and Fig. 9b). This indicates that the wavebreaking region was still present, although retreated and extended upward. Conversely, on the eastern slopes of the SYM at 0000 PDT (Fig. 12n) the lee slope jet intensifies in resonance with the intensification of downslope winds on the southern slopes of the San Rafael Mountains that extend above the inversion layer over the SYV.

At 0200 PDT (Figs. 12e–o) winds weakened over the western SYM (across RHWC1), including the Santa Barbara channel (Fig. 12e), and significantly decreased at the SWEX-site (Fig. 12j), while the lee slope jet maintained strong on the slopes of the San Rafael Mountains and eastern SYM across Montecito (across MOCI1, Fig. 12o). Simulations indicated that the lee slope jet significantly weakened in the foothills of the SYM after 0500 PDT in all longitudes (not shown).

6. Summary and conclusions

SWEX-P was a pilot study in SB County designed to obtain meteorological vertical profiles during a significant Sundowner event (28–29 April 2018), and a unique opportunity to examine driving mechanisms and assess the skill of the WRF Model (1-km grid spacing) in simulating the Sundowners' main characteristics. The synoptic forcing was characterized by a midtroposphere trough that moved across Northern California and created strong pressure gradients at low levels favoring intense offshore (cross-mountain) winds leeward of the SYM. This event was associated with observed differences in sea level pressure between Santa Maria and Santa Barbara airports with maximum magnitude of 25.0 hPa during the evening of 28 April.

SWEX-P provided observational evidence that Sundowners exhibit characteristics of nocturnal downslope windstorms that are controlled by the following main mechanisms: (i) stratification of the boundary layer in the slopes of the SYM; (ii) evolution and intermittence of a nocturnal lee slope jet; (iii) self-induced critical layers caused by mountain-wave breaking; (iv) possible interactions with the offshore coastal jet (particularly in the western portion of the SYM); (v) influence of the MBL on temperature, humidity and winds during daytime and on the elevation of the jet during night time on the coast and foothills of the SYM; and (vi) interactions between mountain flows (downslope winds in the San Rafael Mountains), especially important in the eastern portion of the SYM. These observations were critical in validating the main hypotheses postulated with models (Cannon et al. 2017; Smith et al. 2018a,b; Duine et al. 2019).

During daytime, the MBL and onshore winds influenced circulation in the foothills of SYM and coastal areas over central and eastern parts of the SYM. During the evening, Sundowners exhibited a remarkable spatiotemporal variability; SWEX-P characterized the eastward propagation of the onset of strong nocturnal northerly (cross-mountain) winds (Smith et al. 2018b), and identified significant east–west differences in wind speed and gusts between stations at similar elevations. The strongest winds and gusts were generally observed west of the SYM. The relatively cool temperatures in the western portion of the domain is consistent with the strong influence of the coastal jet (Rahn et al. 2014). Thus, this event seems representative of the ''Gaviota-type'' of Sundowner described in Smith et al. (2018a). However, it is worth noticing that previous studies (Cannon et al. 2017; Sukup 2013; Duine et al. 2019) have shown that Sundowners can be stronger in the eastern sector of the SYM and likely independent of the coastal jet.

In the presence of a coastal jet, strong winds are observed in the western slopes of the SYM. This explains the dominant effect of the western slopes of the SYM on the climatology discussed in Smith et al. (2018b) and the strongest relationships they found between Sundowners and pressure differences between Santa Maria (KSMA) and Santa Barbara (KSBA). Additional studies are necessary to properly address these issues, including the

seasonalityofSundownersandgalewindsintheeasternSYM.

SWEX-P identified strong relationships between the intensification of the nocturnal lee slope jet and gusty winds leeward of the SYM. At the SWEX-P site, the jet was strongest around sunset, when the abrupt radiative cooling enhanced stability in the SYM slopes and in the SYV. Moreover, mountain wave breaking played a critical role in the dynamics of the lee slope jet and intensification of wind speeds leeward of the SYM.

Another relevant result was the weakening of the lee jet (possibly due to the increase in mechanical turbulence and mixing with air at ground level) and reintensification a few hours later (around 0200 PDT). The reintensification of the jet was associated with high wind gusts at ground level at several stations downwind of the SYM. Observations suggest that this secondary peak in winds was not associated with wave breaking. Simulations indicate that this secondary peak was not uniform in the region.

Adiabatic warming, temperature advection and turbulent mixing are important processes influencing temperature tendencies in all locations. Given these issues, we acknowledge the fact that this particular Sundowner event was not characterized by a ramp in temperature for most stations, but by the increase in gusts and decrease in specific humidity with impacts to relative humidity on the slopes of the SYM. While the increase of a few degrees in temperature was observed at some sites during the peak of the winds, temperatures around sunset were not remarkably high, contrasting with anecdotal definitions of these events, some based on episodes that occurred during summer when the lower troposphere is much warmer. This clearly indicates the need for a more adequate definition of Sundowners that is less subjective and properly accounts for the most remarkable characteristics of the phenomenon, including the presence of the lee slope jet and mountain waves, as well as the environment where they occur. Evidently, this definition requires systematic observations of profiles of temperature, humidity, and winds at adequate spatial and temporal resolutions. This can be solely accomplished with a comprehensive field campaign.

WRF captured well mesoscale characteristics of winds, while biases in wind speeds varied according to location. The onset of the nocturnal lee slope jet and high-amplitude mountain wave at the SWEX site were well simulated, providing further confidence that the experiment location was in the supercritical region of the lee of the SYM, and below the wave-breaking region. Our skill assessment indicated that WRF was capable of capturing tendencies in sea level pressure between KSBA and KSMA; however, this criteria alone cannot identify spatiotemporal variabilities in the winds and gusts on mesoscale that appeared largely linked to the behavior of the nocturnal lee slope jet. These results demonstrated that an adequate network of profilers and towers upslope and downslope of the mountains is necessary to further understand driving mechanisms and to adequately assess the skill of WRF in simulating downslope windstorms.

Acknowledgments. This research was supported by the Integrative and Collaborative Education and Research (ICER) program, from the National Science Foundation (ICER–1664173). SWEX-P was funded by UCSBResearch Faculty Grant. Authors thank the Santa Barbara County Fire Department for the logistic support for the realization of SWEX and the NWS LOX for the timely forecasts. Comments and suggestions by Jimmy Dudhia, Forest Cannon, and Maria A. Silva Dias for the design of SWEX-P are much appreciated.

REFERENCES

Blier, W., 1998: The Sundowner winds of Santa Barbara, California. Wea. Forecasting, 13, 702–716, https://doi.org/10.1175/1520-0434(1998)013,0702:TSWOSB.2.0.CO;2.

Cannon, F., L. M. V. Carvalho, C. Jones, T. Hall, D. Gomberg, J. Dumas, and M. Jackson, 2017: WRF simulation of downslope wind events in coastal Santa Barbara County. Atmos. Res., 191, 57–73, https://doi.org/10.1016/j.atmosres.2017.03.010.

Cao, Y., and R. G. Fovell, 2016: Downslope windstorms of San Diego County. Part I: A case study. Mon. Wea. Rev., 144, 529–552, https://doi.org/10.1175/MWR-D-15-0147.1.

——, and ——, 2018: Downslope windstorms of San Diego County. Part II: Physics ensemble analyses and gust forecasting. Wea. Forecasting, 33, 539–559, https://doi.org/ 10.1175/WAF-D-17-0177.1.

Clements, C. B., and A. J. Oliphant, 2014: The California State University Mobile Atmospheric Profiling System: A facility for research and education in boundary layer meteorology. Bull. Amer. Meteor. Soc., 95, 1713–1724, https://doi.org/ 10.1175/BAMS-D-13-00179.1.

Dee, D. P., and Coauthors, 2011: The ERA-Interim reanalysis: Configuration and performance of the data assimilation system. Quart. J. Roy. Meteor. Soc., 137, 553–597, https://doi.org/10.1002/qj.828.

Dorman, C. E., and C. D. Winant, 2000: The structure and variability of the marine atmosphere around the Santa Barbara channel. Mon. Wea. Rev., 128, 261–282, https://doi.org/ 10.1175/1520-0493(2000)128,0261:TSAVOT.2.0.CO;2.

Draxler, R. R., 1999: HYSPLIT4 user's guide. NOAA Tech. Memo. ERLARL-230,NOAAAirResourcesLaboratory,SilverSpring, MD, 38 pp., www.arl.noaa.gov/documents/reports/arl-230.pdf.

Duine, G. J., C. Jones, L. M. V. Carvalho, and R. Fovell, 2019: Simulating Sundowner winds in coastal Santa Barbara: Model validation and sensitivity. Atmosphere, 10, 155, https://doi.org/10.3390/atmos10030155.

Durran, D. R., 1990: Mountain waves and downslope winds. Atmospheric Processes over Complex Terrain, Meteor. Monogr., No. 23, Amer. Meteor. Soc., 59–81.

——, 2003: Downslope winds. Encyclopedia of Atmospheric Sciences, G. North, J. Pyle, and F. Zhang, Eds., Elsevier, 644–650.

——, and J. B. Klemp, 1987: Another look at downslope winds. Part II: Nonlinear amplification beneath wave-overturning layers. J. Atmos. Sci., 44, 3402–3412, https://doi.org/10.1175/ 1520-0469(1987)044,3402:ALADWP.2.0.CO;2.

Fovell, R., and A. Gallagher, 2018: Winds and gusts during the Thomas fire. Fire, 1, 47, https://doi.org/10.3390/fire1030047.

Gallus, W. A., Jr., and J. B. Klemp, 2000: Behavior of flow over step orography. Mon. Wea. Rev., 128, 1153–1164, https://doi.org/10.1175/1520-0493(2000)128,1153:BOFOSO.2.0.CO;2.

Grachev, A. A., L. S. Leo, S. Di Sabatino, H. J. S. Fernando, E. R. Pardyjak, and C. W. Fairall, 2016: Structure of turbulence in katabatic flows below and above the wind-speed maximum. Bound.-Layer Meteor., 159, 469–494, https://doi.org/10.1007/s10546-015-0034-8.

Grubisic´, V., and B. J. Billings, 2007: The intense lee-wave rotor event of Sierra Rotors IOP 8. J. Atmos. Sci., 64, 4178–4201, https://doi.org/10.1175/2006JAS2008.1.

——, and ——, 2008: Summary of the Sierra Rotors Project wave and rotor events. Atmos. Sci. Lett., 9, 176–181, https://doi.org/10.1002/asl.200.

Hatchett, B. J., C. M. Smith, N. J. Nauslar, and M. L. Kaplan, 2018: Brief communication: Synoptic-scale differences between Sundowner and Santa Ana wind regimes in the Santa Ynez mountains, California. Nat. Hazard Earth Syst. Sci., 18, 419–427, https://doi.org/10.5194/nhess-18-419-2018.

Hughes, M., and A. Hall, 2010: Local and synoptic mechanisms causing Southern California's Santa Ana winds. Climate Dyn., 34, 847–857, https://doi.org/10.1007/S00382-009-0650-4.

Iacono, M. J., J. S. Delamere, E. J. Mlawer, M. W. Shephard, S. A. Clough, and W. D. Collins, 2008: Radiative forcing by longlived greenhouse gases: Calculations with the AER radiative transfer models. J. Geophys. Res., 113, D13103, https://doi.org/10.1029/2008JD009944.

Jiang,Q., andJ.D. Doyle,2008: Diurnalvariationof downslope winds inOwensValley during the Sierra RotorExperiment. Mon. Wea. Rev., 136, 3760–3780, https://doi.org/10.1175/2008MWR2469.1.

Jones, C., F. Fujioka, and L. M. V. Carvalho, 2010: Forecast skills of synoptic conditions associated with Santa Ana winds in Southern California. Mon. Wea. Rev., 138, 4528–4541, https://doi.org/10.1175/2010MWR3406.1.

Klemp, J. B., and D. R. Lilly, 1975: The dynamics of wave-induced downslope winds. J. Atmos. Sci., 32, 320–339, https://doi.org/10.1175/1520-0469(1975)032,0320:TDOWID.2.0.CO;2.

Kolden, C., and J. Abatzoglou, 2018: Spatial distribution of wildfires ignited under katabatic versus non-katabatic winds in Mediterranean Southern California USA. Fire, 1, 19, https://doi.org/10.3390/fire1020019.

Lawson, J., and J. Horel, 2015: Analysis of the 1 December 2011 Wasatch downslope windstorm. Wea. Forecasting, 30, 115–135, https://doi.org/10.1175/WAF-D-13-00120.1.

Nakanishi, M., and H. Niino, 2006: An improved Mellor–Yamada level-3 model: Its numerical stability and application to a regional prediction of advection fog. Bound.-Layer Meteor., 119, 397–407, https://doi.org/10.1007/s10546-005-9030-8.

Rahn, D. A., T. R. Parish, and D. Leon, 2014: Coastal jet adjustment near Point Conception, California, with opposing wind in the bight. Mon. Wea. Rev., 142, 1344–1360, https://doi.org/10.1175/MWR-D-13-00177.1.

Ryan,G.,1996:DownslopewindsofSantaBarbara,California.NOAA Tech. Memo. NWS WR-240, 44 pp., https://www.weather.gov/media/wrh/online_publications/TMs/TM-240.pdf.

Skamarock, W. C., and Coauthors, 2008: A description of the Advanced Research WRF version 3. NCAR Tech. Note NCAR/TN-4751STR, 113 pp., https://doi.org/10.5065/D68S4MVH.

Smith, C. M., B. J. Hatchett, and M. L. Kaplan, 2018a: Characteristics of Sundowner winds near Santa Barbara, CA, from a dynamically downscaled climatology: Environment and effects aloft and offshore. J. Geophys. Res. Atmos., 123, 13092–13 110, https://doi.org/10.1029/2018JD029065.

——, ——, and ——, 2018b: Characteristics of Sundowner winds near Santa Barbara, California, from a dynamically downscaled climatology: Environment and effects near the surface. J. Appl. Meteor. Climatol., 57, 589–606, https://doi.org/ 10.1175/JAMC-D-17-0162.1.

Smith, R. B., 1979: The influence of mountains on the atmosphere. Advances in Geophysics, Vol. 21, Academic Press, 87–230, https://doi.org/10.1016/S0065-2687(08)60262-9.

——, 1985: On severe downslope winds. J. Atmos. Sci., 42, 2597–2603, https://doi.org/10.1175/1520-0469(1985)042,2597:OSDW.2.0.CO;2.

Stein, A. F., R. R. Draxler, G. D. Rolph, B. J. B. Stunder, M. D. Cohen, and F. Ngan, 2015: NOAA's HYSPLIT atmospheric transport and dispersion modeling system. Bull. Amer. Meteor. Soc., 96, 2059–2077, https://doi.org/10.1175/BAMSD-14-00110.1.

Stull, R. B., 1988: An Introduction to Boundary Layer Meteorology. Kluwer Academic, 666 pp.

Sukup, S., 2013: Extreme northeasterlywind eventsinthe hillsabove Montecito, California. Western Region Tech. Attachment NWS WR-1302, National Weather Service Western Region, Salt Lake City, UT, 21 pp.

Thompson, G., M. Tewari, K. Ikeda, S. Tessendorf, C. Weeks, J. Otkin, and F. Y. Kong, 2016: Explicitly-coupled cloud physics and radiation parameterizations and subsequent evaluation in WRF high-resolution convective forecasts. Atmos. Res., 168, 92–104, https://doi.org/10.1016/j.atmosres.2015.09.005.

Tiedtke, M., 1989: A comprehensive mass flux scheme for cumulus parameterization in large-scale models. Mon. Wea. Rev., 117, 1779–1800, https://doi.org/10.1175/1520-0493(1989)117,1779:ACMFSF.2.0.CO;2.

Turton, J. V., A. Kirchgaessner, A. N. Ross, and J. C. King, 2017: Does high-resolution modellingimprovethe spatial analysisof fohn flow over the Larsen C Ice Shelf? Weather, 72, 192–196, https://doi.org/10.1002/wea.3028.

Vosper, S. B., 2004: Inversion effects on mountain lee waves. Quart. J. Roy. Meteor. Soc., 130, 1723–1748, https://doi.org/10.1256/qj.03.63.

Whiteman, C. D., 2000: Mountain Meteorology: Fundamentals and Applications. Oxford University Press, 355 pp.

Zhang, C., Y. Wang, and K. Hamilton, 2011: Improved representation of boundary layer clouds over the Southeast Pacific in ARW-WRF using a modified Tiedtke cumulus parameterization scheme. Mon. Wea. Rev., 139, 3489–3513, https:// doi.org/10.1175/MWR-D-10-05091.1.